Video Article

Direct Imaging of Laser-driven Ultrafast Molecular Rotation

Kenta Mizuse[1], Romu Fujimoto[1], Nobuo Mizutani[2], Yasuhiro Ohshima[1,3]

[1]Department of Chemistry, Tokyo Institute of Technology

[2]Equipment Development Center, Institute for Molecular Science

[3]Department of Photo-molecular Science, Institute for Molecular Science

Correspondence to: Kenta Mizuse at mizuse@chem.titech.ac.jp, Yasuhiro Ohshima at ohshima@chem.titech.ac.jp

URL: https://www.jove.com/video/54917
DOI: doi:10.3791/54917

Keywords: Chemistry, Issue 120, femtochemistry, ultrafast phenomena, coherent control, velocity-map imaging, slice imaging, pump-probe experiment, rotational wave packet, intense laser field, molecular dynamics, molecular alignment, femtosecond laser, molecular physics

Date Published: 2/4/2017

Citation: Mizuse, K., Fujimoto, R., Mizutani, N., Ohshima, Y. Direct Imaging of Laser-driven Ultrafast Molecular Rotation. *J. Vis. Exp.* (120), e54917, doi:10.3791/54917 (2017).

Abstract

We present a method for visualizing laser-induced, ultrafast molecular rotational wave packet dynamics. We have developed a new 2-dimensional Coulomb explosion imaging setup in which a hitherto-impractical camera angle is realized. In our imaging technique, diatomic molecules are irradiated with a circularly polarized strong laser pulse. The ejected atomic ions are accelerated perpendicularly to the laser propagation. The ions lying in the laser polarization plane are selected through the use of a mechanical slit and imaged with a high-throughput, 2-dimensional detector installed parallel to the polarization plane. Because a circularly polarized (isotropic) Coulomb exploding pulse is used, the observed angular distribution of the ejected ions directly corresponds to the squared rotational wave function at the time of the pulse irradiation. To create a real-time movie of molecular rotation, the present imaging technique is combined with a femtosecond pump-probe optical setup in which the pump pulses create unidirectionally rotating molecular ensembles. Due to the high image throughput of our detection system, the pump-probe experimental condition can be easily optimized by monitoring a real-time snapshot. As a result, the quality of the observed movie is sufficiently high for visualizing the detailed wave nature of motion. We also note that the present technique can be implemented in existing standard ion imaging setups, offering a new camera angle or viewpoint for the molecular systems without the need for extensive modification.

Video Link

The video component of this article can be found at https://www.jove.com/video/54917/

Introduction

For a deeper understanding and better use of the dynamic nature of molecules, it is essential to clearly visualize molecular motions of interest. Time-resolved Coulomb explosion imaging is one of the powerful approaches to achieve this objective[1,2,3]. In this approach, the molecular dynamics of interest are initiated by a pump ultrashort laser field and are then probed by a time-delayed probe pulse. Upon probe irradiation, molecules are multiply ionized and broken into fragment ions due to the Coulomb repulsion. The spatial distribution of the ejected ions is a measure of the molecular structure and spatial orientation at the probe irradiation. A sequence of measurement scanning the pump-probe delay time leads to the creation of a molecular movie. It is noteworthy that, for the simplest case – diatomic molecules – the angular distribution of the ejected ions directly reflects the molecular axis distribution (*i.e.,* the squared rotational wave function).

With regard to the pump process, recent progress in the coherent control of molecular motion using ultrashort laser fields has led to the creation of highly controlled rotational wave packets[4,5]. Furthermore, the direction of rotation can be actively controlled by using a polarization-controlled laser field[6,7,8]. It has therefore been expected that a detailed picture of molecular rotation, including wave natures, could be visualized when the Coulomb explosion imaging technique is combined with such a pump process[9,10,11,12,13]. However, we sometimes encounter experimental difficulties associated with the existing imaging methods, as mentioned below. The purpose of this paper is to present a new way of overcoming these difficulties and of creating a high-quality movie of molecular rotational wave packets. The first experimental movie of molecular rotation taken with the present method, along with its physical implications, were presented in our previous paper[11]. The background of development, the detailed theoretical aspect of the present imaging technique, and a comparison with other existing techniques will be given in a forthcoming paper. Here, we will mainly focus on the practical and technical aspects of the procedure, including the combination of the typical pump-probe optical setup and the new imaging apparatus. As in the previous paper, the target system is unidirectionally rotating nitrogen molecules[11].

The main experimental difficulty of the existing imaging setup, schematically shown in **Figure 1**, has to do with the position of the detector, or the camera angle. Because the rotational axis coincides with the laser propagation axis[6,7,8] in laser-field-induced molecular rotation, it is not practical to install a detector along the rotational axis. When the detector is installed so as to avoid laser irradiation, the camera angle corresponds to a side observation of rotation. In this case, it is impossible to reconstruct the original orientation of molecules from the projected (2D) ion image[14]. A 3D imaging detector[14,15,16,17,18,19], with which the arrival time to the top detector and the ion impact positions can be measured, offered a unique way to directly observe molecular rotation using Coulomb explosion imaging[10,12]. However, the acceptable ion counts per laser shot are low (typically < 10 ions) in the 3D detector, meaning that it is difficult to create a long movie of molecular motion with high image quality[14].

The dead time of the detectors (typically ns) also affects the image resolution and imaging efficiency. It is also not a simple task to make a good pump-probe beam overlap by monitoring a real-time ion image with a laser repetition rate of <~1 kHz. Although several groups have observed rotational wave packets using the 3D technique, the spatial information was limited and/or direct, and a detailed visualization of wave nature, including complicated nodal structures, was not achieved[10,12].

The essence of the new imaging technique is the use of the "new camera angle" in **Figure 1**. In this configuration, laser beam exposure to a detector is avoided while the 2D detector is parallel to the rotational plane, leading to the observation from the rotational axis direction. The slit allows only the ion in the rotational plane (the polarization plane of the laser pulses) to contribute to an image. A 2D detector, which offers a higher count rate (typically ~100 ions) than a 3D detector, can be used. The setup of the electronics is simpler than in the case of 3D detection, while the measurement efficiency is higher. Time-consuming mathematical reconstruction, such as Abel inversion[14], is also not needed to extract angular information. These features lead to the easy optimization of the measurement system and to the production of high-quality movies. A standard 2D/3D charged-particle imaging apparatus can be easily modified to the present setup without the use of expensive equipment.

Protocol

NOTE: Through this protocol, we clarify what we actually did to develop the present method. Exact parameters, including chamber and optical setup design and the sizes and types of the parts, are not always essential to apply the present system to the reader's apparatus. The essence of the procedures will be given as notes in each step.

1. Construction of a 2D-slice Imaging Apparatus

NOTE: Throughout this step, all the commercially available parts and equipment, such as a vacuum pump and a detector, are installed according to the manufacturer's instructions or user's manuals.

1. As in the construction of a typical 2D/3D ion imaging apparatus[14], design and build a differentially pumped vacuum chamber that has enough space to accommodate a pulsed valve, molecular beam skimmers, ion optics (a stack of 100 mm rings with a 50 mm hole), an off-axis ion imaging unit (a pulsed repeller electrode and a stack of microchannel plates backed by a phosphor screen), and an ion flight tube (>200 mm drift region).
2. Attach the pulsed valve to the chamber partition using four threaded posts (15 cm, Φ12 mm), for which bolt holes on the partition are concentric to the chamber. Install the molecular beam skimmers to the chamber partition directly in front of the nozzle using a keep plate.
   NOTE: In the construction of an ion imaging apparatus, it is essential that the molecular beam axis and laser beam axis intersect at the axis of the ion optics. To achieve this, it is convenient to define the molecular beam axis as a source chamber axis. Step 1.2 is for this purpose. In addition, the skimmer holes should be in line with the nozzle of the valve, ensuring that the center of the molecular beams can enter the differentially pumped stage through a skimmer. It is also important to consider the weight of the pulsed valve; hence, sufficiently thick threaded posts must be used to connect the pulsed valve to the partition wall. Maintain the 15 cm distance between the nozzle and the partition in order to avoid the reflection effect of gas and skimmer interference[20].
3. Install ion optics to the final stage of the differentially pumped chamber, as in a typical ion imaging setup[21].
   NOTE: This step is carried out as follows: The threaded mounting posts are screwed to the chamber partition. On the posts, a stack of ion optics is locked in place with nuts. Because the bolt holes for the posts are concentric to the chamber, the axis of the ion optics coincides with that of the molecular beam.
4. Install the optical glass windows (1 mm thickness, 25 mm diameter, fused silica) by placing a P16 O-ring between a vacuum flange with a hole and a window, so that laser pulses can intersect the molecular beam.
   NOTE: Through these windows, laser pulses can access the middle of the first and the second ion electrodes and intersect the axis of ion optics.
5. Construct an off-axis ion imaging unit (**Figure 2**).
   NOTE: Throughout this step, refer to **Figure 2** to verify the 3-dimensional arrangement of the unit. All the electrode parts (the ion detector and the repeller) are mounted to the 100 mm baseplate with PEEK bolts, while the other parts are mounted with stainless bolts. The essence is to mount a 2D imaging detector in the ion drift region so that its detector surface is parallel to the ion optics axis and perpendicular to the laser propagation axis. Of course, all the parts to be used in high-voltage should be electrically isolated. We recommend that the distance between the ion optics (flight) axis and the detector surface is a few mm (in the present case, 5 mm). With a longer distance, it will take more time to push the ions to a detector, and a shorter distance might result in discharge between the MCP surface and the pulsed repeller.
   1. Observe the edge of the slit blades (100 mm length) with an optical microscope (~30X) and/or an optical comparator and confirm that there are no dents or scratches larger than 30 µm located at edge of the slit blades.
      NOTE: The slit blades should be mounted in parallel, and no dents and scratches are acceptable. The deviation from the parallel leads to the inhomogeneity of ion detection. A defect of the blade degrades an observed image (see the discussion section).
   2. Using small mounting claws, attach the slit blades to the slit blade holder, which consists of a pair of 122.4 mm aluminum plates connected with a spring, as in a clothespin. Also insert a tapered aluminum rod into the "clothes pin."
      NOTE: The slit blades are mounted on the knob side (point of effort) of the clothespin. When a tapered aluminum rod of a sharpened pencil-like shape is inserted into the pinching side (point of action) of the clothespin, the slit width becomes larger with increasing depth insertion of the tapered rod (See **Figure 2B**). Steps 1.5.2-1.5.4 are for the construction of the slit, the width of which can be tuned during the imaging measurement. If width tuning is not needed, just install the slit blade ~10 cm upstream of the ion beam from the detector using suitable mounting parts as metal claws and go to step 1.5.5.
   3. Attach the tapered aluminum rod to the linear motion vacuum feedthrough (micrometer/bellows-based, ICF70 size) and mount the slit holder and base to the vacuum side plane of the feedthrough.
   4. Install the slit unit constructed above onto an ICF70 vacuum port that is perpendicular both to the detector axis and to the ion flight axis.
      NOTE: The position is ~10 cm upstream of the ion beam from the center of the detector.
   5. Set the slit width to 1 ± 0.1 mm using a micrometer.

NOTE: For example, the use of a 1 mm slit for the 50-mm Newton sphere (ion cloud) corresponds to 2% slicing, which is higher in resolution than the standard slice technique[22]. The slit width determines the slice resolution; however, smaller widths lead to weaker signals.

6. Install a pulsed repeller electrode of rectangular (115 mm x 160 mm x 3 mm) stainless plate, as in **Figure 2**.
   NOTE: The pulsed repeller should be parallel to the detector to ensure the homogeneity of the pulsed electric field between them.
7. Install a position-sensitive ion detector consisting of a stack of microchannel plates backed by a phosphor screen so that it is parallel to the pulsed repeller; follow standard mounting procedure[14,23].
8. Install a flange-mounted vacuum viewport with a copper gasket to the back of the phosphor screen.

6. Wire the ion optics to high-voltage power supplies and the parts of the detector (a pulsed repeller, microchannel plates, and a phosphor screen) to pulsed high-voltage supplies (~50 ns rise/fall time) via current feedthroughs.
   NOTE: Care should be taken to ensure that any cables do not interrupt the observation of the phosphor screen through the viewport.
7. Connect the pulsed valve to the gas inlet (3% N_2 gas in He; total pressure of 3 MPa) with a stainless tube and to the valve controller with a pair of coated copper wires.
   NOTE: Both connections pass through vacuum feedthroughs.
8. Turn the vacuum pumps on and set the pressure of the imaging detector chamber lower than 10^{-4} Pa, even when the pulsed valve is in operation.
   NOTE: A higher pressure might lead to the damage of the high-voltage electrode and detectors. When the pressure is higher, larger pumps or the reduction of the repetition rate of the valve is required. Using the present chamber and pulsed valve, a nitrogen molecular beam with a rotational temperature below 6 K can be generated[11]. At this rotational temperature, 99% of the molecules are in the $J \leq 2$ state (J is the rotational quantum number).

2. Construction of a Pump-probe Optical Setup

NOTE: For this step, see **Figure 3** to understand where and how the following steps are carried out. The purpose of this step is to create three collinear fs pulses from a commercial Ti:sapphire laser amplifier for the pump-probe experiment[11]. The first pulse was for molecular alignment (linearly polarized, center wavelength of 820 nm, peak intensity <30 TW/cm^2), the second was for the direction control (a delayed replica of the first one, except for the linear polarization +45° tilted from the polarization axis of the first pulse), and the third was the Coulomb explosion imaging probe (circularly polarized, 407 nm, 100 fs, 600 TW/cm^2). Throughout this step, all the commercially available parts and equipment, such as a polarization checker and an optical stage, are installed and used according to the manufacturer's instructions or user's manuals.

NOTE: Throughout this step, all the optical components are installed and used according to the standard procedures of optical experiments and the manufacturer's guide for optics. All the turning and dichroic mirrors used are dielectric multilayer mirrors in order to avoid laser power loss during the many reflections in the optical path. Some of the optics and crystals used are shown in the material list for this article.

1. Turn the femtosecond laser (Ti:sapphire amplifier) system on and acquire a laser output of more than 1.5 mJ/pulse, a ~35 fs duration, a 820 nm center wavelength, and a 500 Hz repetition rate.
2. **Prepare an optical path of the probe (imaging) pulse[10,11,12].**
   1. Install a nonlinear crystal (BBO, type I, 0.2-mm thickness, 29.2°, for the second-harmonic generation of an 820-nm light) in the 820-nm optical path to obtain the second harmonics (>0.2 mJ) of the fundamental 820-nm laser output. Use the generated second harmonics (407 nm light) as a probe pulse after it is reflected by dichroic mirrors and separated from the fundamental 820 nm light.
   2. Construct an optical path, as shown by the blue line in **Figure 3**. Using beam-steering mirror mounts, align this beam to pass through the center of both windows installed in step 1.4.
      NOTE: The key components consist of an attenuator (the combination of a half-waveplate and a polarizer), a motorized linear stage for delay scanning, and waveplates for polarization tuning.

3. **Prepare an optical path for the pump (rotational excitation) pulses[24,25,26].**
   1. Construct an optical path, as shown by the red line in **Figure 3**, and obtain a pair of time- and polarization-tunable fs pulses.
      NOTE: The residual 820-nm pulse (~1 mJ) after the second-harmonic generation in step 2.2.1, ejected from the dichroic mirror, is used to create these pump pulses. The typical pulse energy of each pump pulse is 0.25 mJ. The key components consist of an attenuator (the combination of a half-waveplate and a polarizer), a 50:50 beam splitter, a manual linear stage for time-delay tuning, waveplates for polarization tuning, and a telescope for the spot-size optimization.
   2. By adjusting the tilt of the mirror mounts in the optical path, align the pair of pump beams to be parallel and make their center pass through the center of both windows installed in step 1.4.
      NOTE: To verify this, an alignment tool, an aluminum block with attached graph paper, is used. The tool can be placed in the same position with high reproducibility using the tapped hole of an optical table. Two screw holes in line are chosen as a guide of the parallel path. As the alignment tool is positioned in one of the holes selected, the beams are aligned so that they hit the same point of the alignment tool. Repeat the positioning of the tool and the alignment of the beam until the beam hits the same point of the tool for both alignment-tool positions. Because the screw holes in the optical table are in line with high precision, these procedures lead to the creation of the parallel beams.

4. **Adjust the polarization states of the pulses.**
   1. Install a polarization checker just before the pulses enter the chamber so that the laser pulses hit the detector of the checker.
   2. Adjust the angle of the waveplates using a rotational optics mount in each optical path. Obtain the circularly polarized probe pulse, the vertically polarized first pump pulse, and the linearly polarized second pump pulse; for the second pump, tilt the polarization plane 45° from that of the first pump.
      NOTE: With the use of a polarization checker, the polarization state of each pulse can be visualized as a polar angle-dependent transmission intensity. To obtain a circular polarization, adjust the waveplate angle to achieve an isotropic image, for example.
   3. Remove the polarization checker from the optical path.

NOTE: The first pump initiates direction-undefined rotation[4,9,10]. At the time of the instantaneous molecular alignment, the second pump is shined to create an asymmetric torque and to start the unidirectional rotation[12,13]. Since a circularly polarized probe pulse ionizes the molecules without angular preference in the polarization plane, it is suitable for an angular distribution measurement.

5. **Find the temporal overlap of each pulse.**
    1. Install a nonlinear crystal (BBO, 0.2 mm thickness, type 2, for the third-harmonic generation of 820-nm light), an optical window that has the same thickness (3 mm) as the sum of the chamber window (1 mm) and the focusing plano-convex lens (2 mm), and a dispersion prism just before the pulses enter the chamber.
    NOTE: A standard procedure to determine the time zero (temporal overlap of the pump and probe pulse) in the pump-probe experiment is to detect a nonlinear response, which is observed only when both the pump and the probe pulse simultaneously interact with a medium. Here, the temporal overlap of the 407 nm probe pulse and the 820 nm pump pulse in the nonlinear crystal leads to a 267 nm generation. We have to estimate the temporal overlap of the beams in the vacuum chamber while step 2.5.1 is carried out before the pulses enter the chamber (and the focusing lens and chamber window). Therefore, to compensate the time delay introduced by the chamber window and the focusing lens, a 3-mm optical window is installed. Two pumps and one probe pass through the window and then the crystal, and they are subsequently dispersed by a prism. Place a sheet of white paper after the prism to detect the generation of the 267-nm third harmonics as a white-blue fluorescence. All the mentioned parts are mounted on an optical holder.
    2. Block the line of pump 2 in **Figure 3** with a beam dumper.
    3. Pressing the move button on a stage controller, scan the motorized stage and find a 267 nm generation.
    NOTE: When the optical path length of the pump and probe pulses are the same within the duration of the laser pulses, a third-harmonics signal appears. This stage position is regarded as time 0, during which both the pump and the probe are simultaneously hitting the molecules.
    4. Block pump 1 and unblock pump 2 (remove the beam dumper).
    5. Scan the µm-based manual stage installed in the pump 2 line and find the position at which the 267 nm emission occurs.
    6. Remove the crystal, the window, and the prism from the optical line.
    NOTE: At this stage, the three pulses are temporarily overlapped at the molecular beam within the laser durations. The time resolution of the setup can be measured as a cross-correlation by monitoring and plotting the 267 nm energy while scanning the motorized stage in the probe path. In the present setup, the full width at half maximum of the correlation function is ~120 fs. The pulse width is optimized to obtain the highest power output of the second harmonics. After the second-harmonic generation, the pulses pass through glass lenses, waveplates, dichroic mirrors, polarizers, and the chamber window, leading to a chirp. Because the group delay dispersion of the materials in the 400-nm region is much larger than in the 800-nm region, we minimize the transmission optics in the probe path. To improve the time resolution, dispersion management, including a chirped mirror system, will be helpful.

3. Setup for a Measurement System

NOTE: Throughout this step, all the commercially available parts and equipment, such as a power supply and delay generators, are installed and used according to the manufacturer's instructions or user's manuals.

1. **Pulse synchronization**
    1. Divide the 80.8 MHz output of a femtosecond oscillator to 500 Hz with a fast frequency-divider, and use this divided output to trigger digital delay generator 1 and a fs amplifier.
    2. Use one of the delayed outputs of delay generator 1 as a trigger for the pulsed valve.
    NOTE: Limit the repetition rate of the valve to maintain acceptable vacuum conditions (less than 10^{-3} Pa, for example). In this case, we set the value to 250 Hz.
    3. Install a fast photodiode equipped with a 400 nm transmission filter just after the beams exit the chamber, and use the output of this diode as a trigger for digital delay generator 2.
    NOTE: The probe pulse is used as a time origin for the ion imaging electronics.
    4. Connect three high-voltage switches to digital delay generator 2 with coaxial cables.

2. Turn all high-voltage power supplies and switches on.
3. **Increase the voltage to the target values.**
    NOTE: The target voltages depend on the size of the apparatus and the system of interest. Typical values in the present case are shown in the caption of **Figure 1**. To obtain undistorted images, fine-tuning the bias voltages is required[13] (see step 4.1.7). A rapid increase in the voltage value might result in the discharge of or damage to the electronics system. We recommend an increase of less than 100 V/s for daily operation and an increase of 100 V/300 s for the first use in a vacuum.
4. **Installation and positioning of the imaging camera**
    1. Install a digital camera equipped with a *f* = 25 mm camera lens on the optical post in front of the vacuum viewport set in step 1.5.5. Ensure that the camera axis is perpendicular to the detector surface. Because the viewport is perpendicular to the floor level, use a water-level guide to align the camera base horizontally relative to the floor.
    NOTE: Fine adjustments of the position are done in a later step.
    2. Install a cooling fan for the camera so that the wind hits the camera from the back.
    3. Cover the region between the camera lens and the vacuum viewport with a curtain so that unwanted light, such as ambient room lighting, does not enter the camera.
    4. Connect the camera to a computer via a USB 3.0 port.
    5. Start the camera control software and maximize the gain of the camera by entering the maximum value in the gain control section of the software.
    6. Set the image size to typically 1,200 x 750 pixels.
    NOTE: Although a larger image size leads to higher resolution, the data rate of the USB 3.0 port limits the acceptable frame rate. At the present settings, more than 250 fps can be achieved, which is high enough to obtain an image for every gas pulse loading (250 Hz).

7. Start capturing images with the camera by clicking the "Grab" button. Manually adjust the position of the camera so that the image covers the entire area of the 2D detector. Fix the camera mount with a bolt.
8. By monitoring a real-time captured image, adjust the focus ring of the camera lens so that the bright ion spot size becomes the minimum.

4. Measurements

NOTE: The measurement method used here is a combination of reported procedures[14,27] and the present imaging setup. Throughout this step, all the commercially available parts and equipment, such as high-voltage electronics, are installed and used according to the manufacturer's instructions or user's manuals.

1. **Finding the signal and optimizing the settings for ion imaging**
   1. Block the pump pulses of the optical system with a beam dumper.
   2. In the middle of the first and the second electrodes of the ion optics, install a plano-convex lens (f = 120 mm) to focus the probe laser pulse to the molecular beam.
   3. Set the time of the high-voltage switches (a digital delay generator output) to the estimated arrival time of the N_2^+ ion, which provides the largest signal intensity under the present gas condition[14,27].
      NOTE: The arrival time can be estimated from the ion optics biases and the distance of flight, along with the mass-to-charge ratio of the target ion[28]. Otherwise, scanning the time is the other solution for detecting a signal.
   4. While monitoring the ion image, adjust the lens position with an xyz-stage and the gas pulse time (a digital delay generator output), and acquire the largest signal (brightest and largest image).
   5. Change the time of the high-voltage switches to the Coulomb exploded N^{2+} channel[14,27].
      NOTE: Because the mass-to-charge ratio of N^{2+} is four times smaller than that of N_2^+, the arrival time of N^{2+} is almost two times faster than that of N_2^+.
   6. Decrease the camera frame rate to ~20 fps and increase the exposure time to 50 ms.
      NOTE: With this setting, the camera image includes the signal for 12 gas pulse loadings. Although this leads to the overlap of some ions, we can easily evaluate and recognize the rough shape of the ion distribution.
   7. Adjust the ion optic biases so that the observed ion distribution becomes an undistorted ellipse.
      NOTE: Decreasing the bias difference between the first and the second electrodes results in the elongation of the vertical direction (ion optics axis) in the present arrangement[29,30]. The third or later optics are used for the fine adjustment of the shape. The distortion of the ellipse degrades the angular resolution reconstructed from the image.

2. **Finding a pump-probe spatial overlap**
   1. Unblock pump 1, removing a beam dumper, but keep pump 2 blocked.
   2. Adjust the telescope to locate the beam waist of the pump pulse in a molecular beam.
      NOTE: Do not change the position of the focusing lens in front of the chamber window, which is optimized for the probe pulse.
      NOTE: This procedure can be accomplished by reflecting the laser beams to the free space under atmospheric pressure just before they enter the vacuum chamber. By measuring the focal length for the same entrance lens, the telescope can be optimized.
   3. Carefully adjust the spot position of the pump beam with high-resolution mirror mount 1 (**Figure 2**), and find the enhanced signal in the ion image due to the pump-probe overlap. Before or after that, set t to ~4 ps by moving a delay stage 600 μm forward. Find the strongly anisotropic image along the pump 1 polarization.
      NOTE: Because the time overlap was roughly optimized in step 2.5, only the spatial overlap needs to be tuned. If the rotational constant or wave packet dynamics are known for the target molecule, an alternative choice is to set the probe delay to an instantaneous molecular alignment time. For example, it could occur at $\Delta t \sim 1/2B$, where Δt is the time difference between the pump and probe pulse and B is the rotational constant in Hz[10,11]. For N_2, ~8.3 ps. At such a time, the pump-probe spatial overlap leads to the ion distribution showing the maximum in the pump polarization direction (vertical in the present case) and the minimum in the perpendicular axis. It is easier to find such an alignment signature compared to the gross enhancement obtained at $\Delta t \sim 0$. With regard to the changing of the Δt, note that, according to the speed of light, a 5 μm movement of the stage corresponds to ~33.356 fs.
   4. Block pump 1 and unblock pump 2.
   5. Repeat step 4.2.3 for pump 2. Find a pump-probe overlap for pump 2 by adjusting high-resolution mirror mount 2 (**Figure 2**) while keeping the optical path of pump 1 unchanged.
      NOTE: Be sure that the polarization of pump 2 is tilted so that the alignment is observed along an oblique direction when the time is set to the alignment time.

3. **Briefly observe the unidirectional rotation dynamics**
   1. Unblock pump 1. Set the time delay between pumps 1 and 2 to the alignment time (*e.g.,* 4.0 ps for a N_2 case[10,11]) with the manual delay stage 1 in **Figure 2**.
   2. Check to determine if the unidirectional rotation can be recognized from camera images as the probe delay is scanned (with a motorized or manual stage).
      NOTE: When all the above procedures are well accomplished, one can see the images in which the brightest region smoothly rotates in one direction as the probe delay is scanned. If such a movie cannot be seen, carefully repeat steps 4.1-4.2. The drift effect of optical mounts sometimes degrades the beam overlap.
      NOTE: According to the speed of light, a 5 μm movement of the stage corresponds to ~33.356 fs. For merely observational purposes, the above-mentioned procedures are sufficient. For the recording and detailed analysis of the motion, go on to the following steps.

4. **Setup measurements**
   1. Increase the camera frame rate to 250 fps and decrease the exposure time to ~4 ms.
      NOTE: One camera frame corresponds to an image for one laser shot/gas pulse loading.
   2. Start the measurement program, which controls the instruments, captures the images, and analyzes and visualizes data.

3. Click the execute button and capture 1,000 images while blocking the pump beams.
4. Numerically fit the summed image with an ellipse and obtain the ellipticity ε and the center of the ellipse (x_0,y_0).
   NOTE: When a raw image has more than one ellipse due to the multiple channels of the Coulomb explosion, limit the region of interest and use only one of the ellipses.
5. Capture 100,000 images while blocking the pump beams and use the obtained image as a probe-only reference.
   NOTE: The signal-to-noise ratio of the probe-only reference image affects the quality of angular distribution. Therefore, a relatively long measurement (~400 s) is taken for this step.

5. **Taking a movie of unidirectional molecular rotation**
   1. Unblock the pump beams.
   2. Set the probe time to a negative value (*t* ~-100 fs; *i.e.,* before the pump beams).
   3. Start the measurement loop, including the following steps
      1. Capture an image. Find the center-of-mass coordinate of each bright ion spot, and binarize the image by assigning "1" to the center of the mass coordinates and "0" to the other pixels[27].
      2. Sum the binarized images for 10,000 camera frames by setting "the number of images" input box of the program to 10,000.
         NOTE: To avoid the saturation effect, set the image depth of the summed image to 16 bits.
      3. Convert the camera coordinate (*x*,*y*) to the polar coordinate using the ellipticity ε determined in step 4.4.4.
         NOTE: This process is completed as follows: In the elliptical region of interest, all the pixel coordinates (*x*,*y*) are converted to their relative polar coordinates *Φ* using the following equation:
         $$\phi = \arctan\left[\frac{(y-y_0)}{\epsilon\,(x-x_0)}\right]$$
         NOTE: This step is equivalent to the image expansion in the vertical direction when converting an ellipse to a circle.
      4. Convert the obtained image to a polar plot in which the angular-dependent signal intensity is plotted as the distance from the origin.
         NOTE: Angle-dependent probability *P*(*Φ*) is calculated using the following equation:
         $$P(\phi) = \frac{(sum\ of\ the\ pixel\ values\ of\ which\ pixels\ are\ in\ \phi\pm 0.5^\circ)}{(number\ of\ pixels\ located\ in\ \phi\pm 0.5^\circ)}$$
      5. Normalize the polar plot, dividing it by that of the probe-only reference.
         NOTE: This step calibrates both the incomplete circular polarization of the probe pulse and the inhomogeneity of the imaging detector.
      6. Move the probe time forward by ~33.356 fs.
         NOTE: A 33.356-fs shift of the probe time corresponds to a 5 μm movement of the motorized linear stage.

   4. Continue the loop until at least one rotational revival period, 1/2*B* (~8.3 ps for N_2), is passed after the pump 2 time.

Representative Results

Figure 4A shows a probe-only raw image of the N^{2+} ion ejected upon probe irradiation (Coulomb explosion), taken for one probe laser shot. Each bright spot corresponds to one ion. **Figure 4B** shows a summed image of 10,000 binarized raw camera images. These images show that our imaging setup can monitor the molecules of all the orientation angles in the polarization plane. **Figure 4C** shows the normalized polar plot corresponding to that of **Figure 4B**. Because the rotational control (pump) pulse was absent, the distribution is isotropic (**Figure 4C** shows a circle).

In **Figure 4B**, a small defect due to detector inhomogeneity can be seen in the bottom of the ellipse. Such a defect always appears in the same position of the image. Therefore, it can be compensated for by normalizing the observed images with a probe-only image (step 4.5.3.7).

Figure 5 shows selected snapshots taken after the irradiation of the two pump pulses. So as to improve understanding, not only the observed ion images, but also the corresponding polar plots and "dumbbell" model pictures are shown as a function of probe time. The polar plots are created in step 4.5.3.5. The dumbbell picture is an overlapped image of dumbbells of various orientation angles, and their weights (opacity) are the observed angular probabilities. The sequence of images forms a clear movie of unidirectional molecular rotation. The wave nature of motion can be seen as the complicated nodal structures and the dispersion, including an "X"-shape formation.

Figure 6 shows an ion image taken with a damaged slit and a photograph of the slit edge with a dent. A small defect largely affects the observed image. In such a case, repeating step 1.5 is required. This fact is also discussed in the discussion section.

Figure 7 shows the raw camera image at the optimized pump-probe overlap condition. By monitoring such a beam overlap signal, the optical paths can be optimized. This leads to a clear movie, as in **Figure 5**.

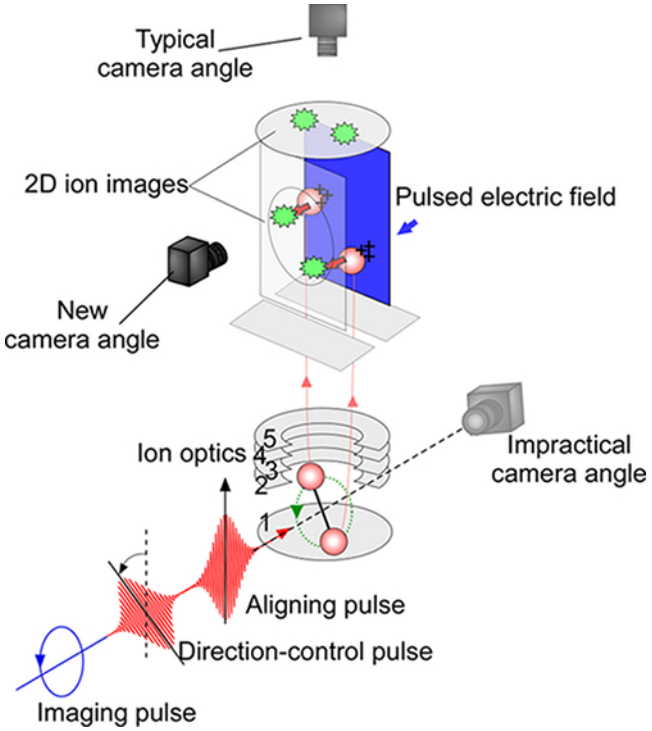

Figure 1: Conceptual diagram of the camera angles in the impractical, typical, and new configurations. In the typical camera angle, a detector is installed to avoid laser exposure, but the ejection angles of ions cannot be reconstructed from the 2D projected image. In the present, new camera angle, the rotational plane (laser polarization plane) is parallel to the detector surface and is therefore suitable for visualizing the rotational motion. Typical bias voltages are 2,500 V, 1,799 V, 1,846 V, 253 V, 0 V, 3,500 V, -800 V, and 4,500 V for ion optics 1, 2, 3, 4, and 5, the pulsed repeller, the microchannel plates, and the phosphor screen, respectively. The ion optics numbering starts at the bottom electrode. Please click here to view a larger version of this figure.

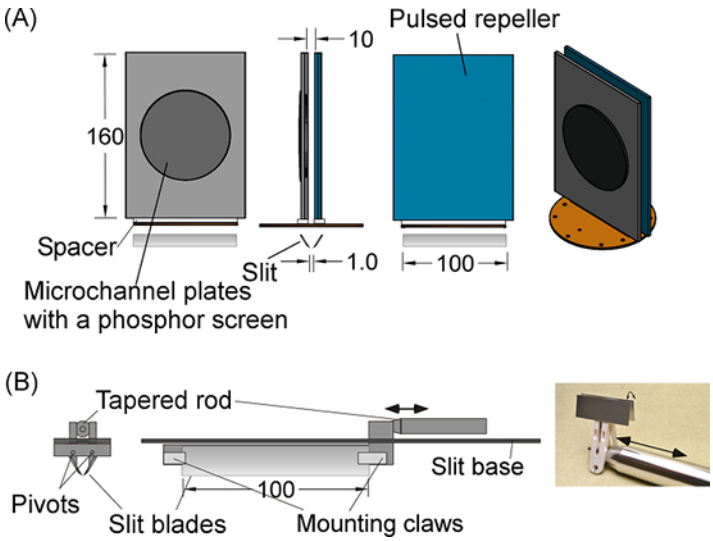

Figure 2: Schematic diagrams of the 2D imaging unit. (**A**) Schematic diagram of the detector assembly. A circle plate colored in orange is a baseplate to which the other parts are mounted with bolts. (**B**) Schematic diagram of the slit assembly. The right picture explains the motion of the slit. The size values are in mm. Please click here to view a larger version of this figure.

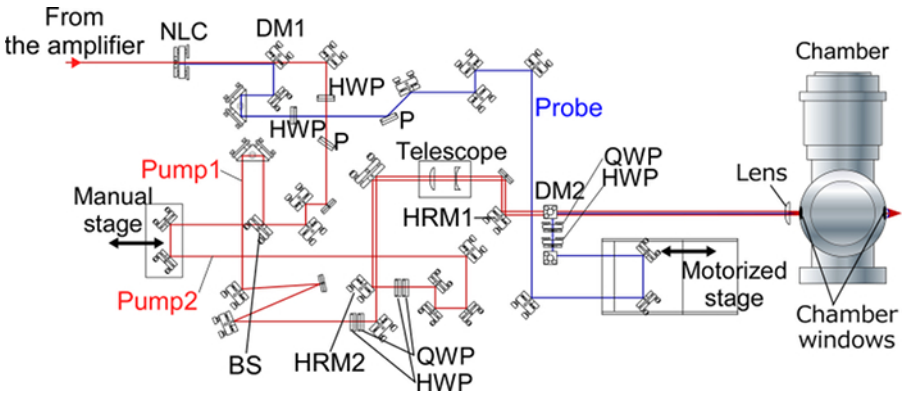

Figure 3: Schematic diagram of the present pump-probe optical setup. The optical paths of the pump pulses for rotational excitation are illustrated by the red lines, while that of the probe (imaging) pulse is shown by the blue line. NLC, nonlinear crystal for second-harmonic generation; HWP, half-waveplate; QWP, quarter-waveplate; DM, dichroic mirror; BS, 50:50 beam splitter; HRM: high-resolution mirror mount. Please click here to view a larger version of this figure.

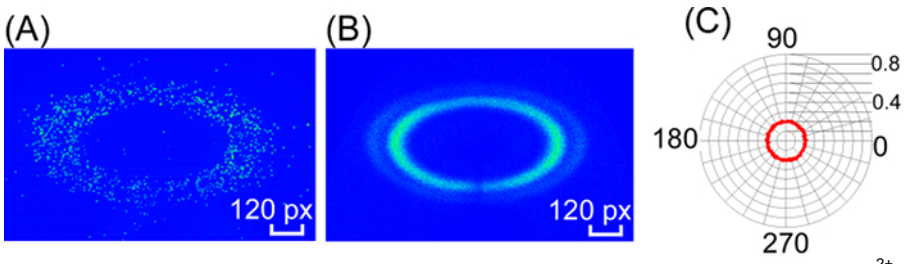

Figure 4: Raw and analyzed Coulomb exploded ion images. (**A**) A typical raw image of N^{2+} taken for one probe shot. (**B**) Summed image for 10,000 binarized camera images. The size of the camera image is 1,200 x 750 pixels. The corresponding real-space size is 80 mm x 50 mm. (**C**) The normalized polar plot constructed from the summed image. In the raw and summed images, false color was added to show the signal intensity. The polar angles in degrees are shown along the circumference. The radial value is an angle-dependent probability (arbitrary unit). Please click here to view a larger version of this figure.

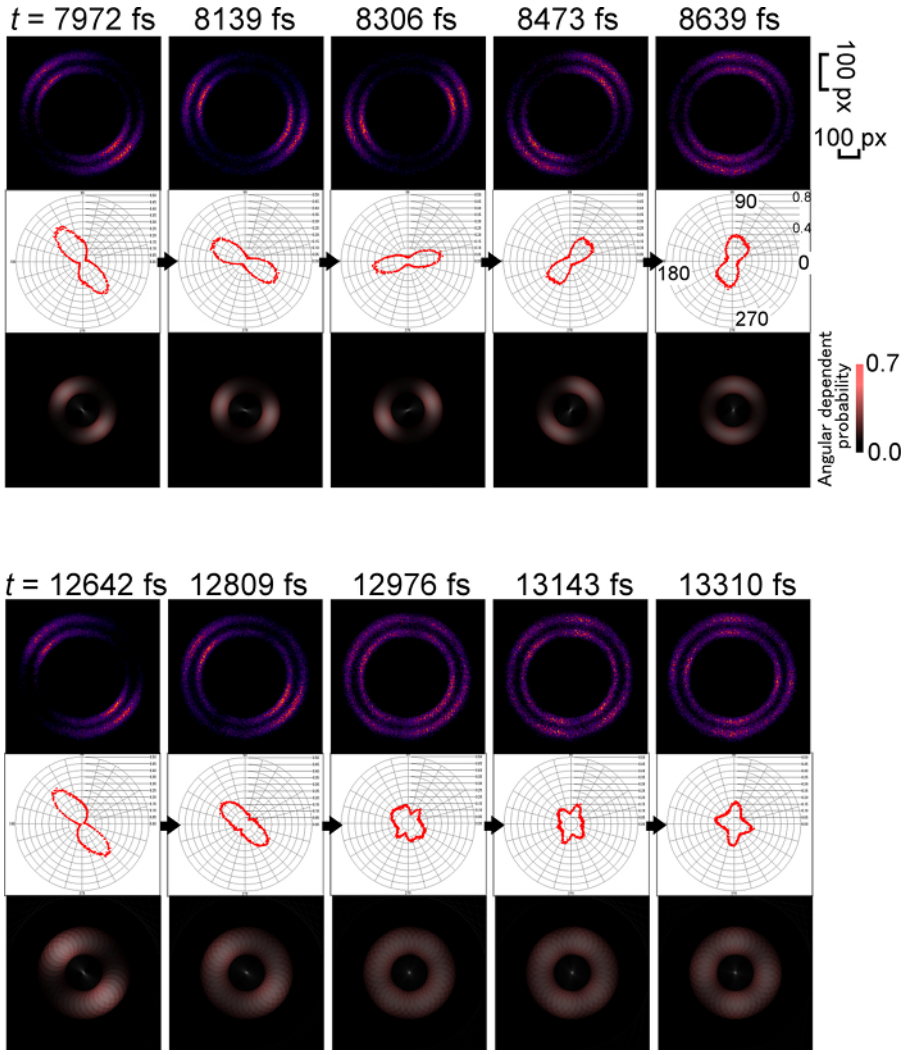

Figure 5: Selected snapshots of the laser-induced rotational wave packet dynamics. In each time delay, the upper panel shows the ion image in which the elliptical shape has been converted to a circle. The middle panel shows the corresponding polar plot. The bottom panel shows a dumbbell model of the angular distribution. This dumbbell picture is an overlapped image of dumbbells from various orientation angles, and their weights (opacity) are the observed angular probabilities. The polar plot uses the same unit and scale as in **Figure 4**. The ion image employs transformed coordinates, as in step 4.5.3.4. Please click here to view a larger version of this figure.

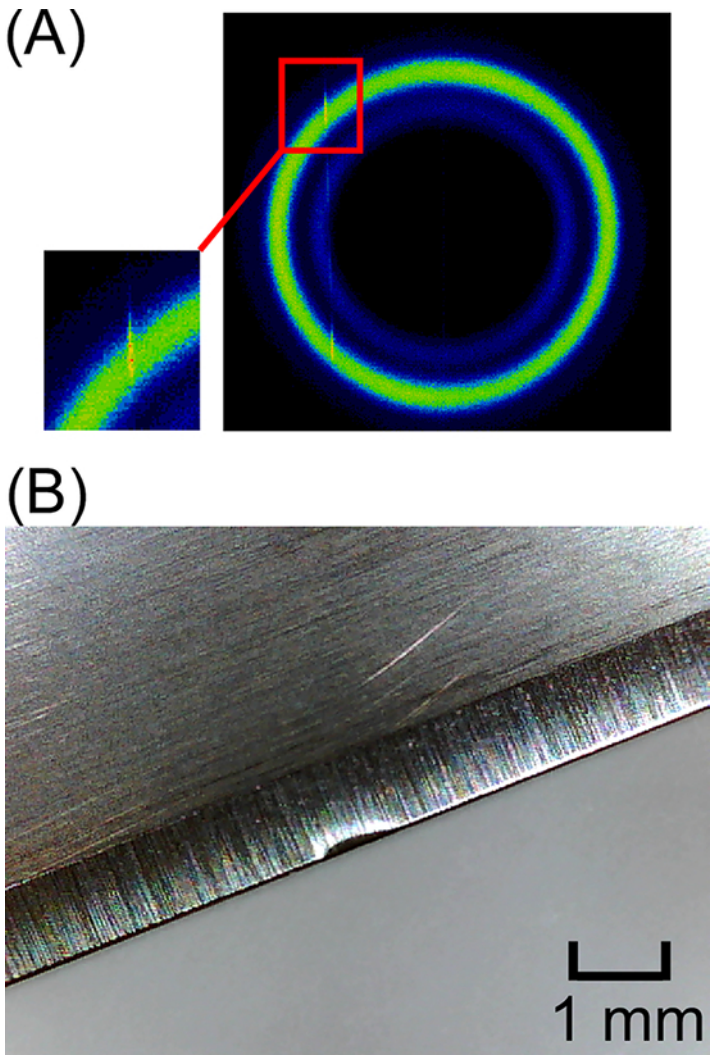

Figure 6: Effect of the slit defect on the experimental ion image. (**A**) Observed probe-only N^{2+} ion image taken with a damaged slit. (**B**) Photograph of the slit edge having a sub-mm dent. Please click here to view a larger version of this figure.

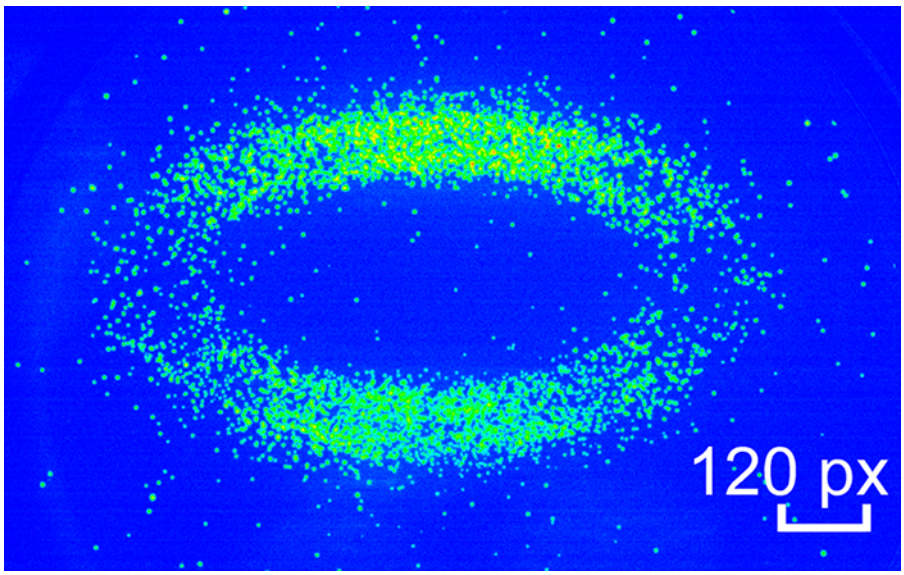

Figure 7: Raw camera image at the optimized pump-probe overlap condition. The probe time is set at t = 4.0 ps after the first pump pulse irradiation. At this time, the maximum degree of molecular alignment is achieved. The size of the camera image is 1,200 x 750 pixels. The corresponding real-space size is 80 mm x 50 mm. Please click here to view a larger version of this figure.

Discussion

The present procedure enables us to capture a real-time movie of molecular rotation with a slit-based 2D imaging setup. Because the observed ions pass through the slit, step 1.5 is one of the critical steps. The edges of the slit blades must be sharp. When there is a small defect, such as a 0.3 mm dent in the slit, a scratch is observed in the ion image (**Figure 6**). In such a case, the slit blade should be polished with 2,000-grit wet sandpaper.

Apart from the unique camera angle shown in **Figure 1**, this method has several advantages over the 3D imaging detector, which was previously the only solution for rotational wave packet imaging.

First, in the present procedure, optical beam alignment can be carried out easily by monitoring raw ion images, as in steps 4.1-4.2. **Figure 7** shows the raw camera image at the optimized pump-probe overlap condition. When the pump-probe beam overlap is lost, anisotropic or enhanced image signatures cannot be seen, as in **Figure 4A**. This fact emphasizes the importance of steps 4.1-4.2 in the present method. Because the spot sizes of the pump and probe beams are on the order of 10 μm, it is generally difficult to find an optimal overlap condition without monitoring real-time images. In the case of a 3D imaging detector, several seconds are required to form an image with sufficient data points (at least 1,000 ions) when a 1,000 Hz or lower repetition-rate laser is employed, because the count rate is limited to a few events per laser shot in the 3D detector. In the present method, on the other hand, the count rate is essentially unlimited, and the number of ions per frame can be increased simply by extending the exposure time. In the present case, more than 1,000 ions are detected within the 50 ms exposure time.

The high count rate of the present method also leads to a shorter data acquisition time. Because the frame rate of the camera is 250 fps, it takes only ~40 s to take one snapshot of the molecular motion at a particular time. For the measurement over the one molecular rotational revival time (~8.4 ps) with a ~33-fs step, the measurement time is only a few hours. This is another advantage, because experimental data would be degraded by the limited long-term stability of the lasers and the entire experimental setup. In our setup, for example, time duration changes with time, partly due to the temperature change in the fs amplifier. A 3-K change within 6 h resulted in the thermal expansion of the amplifier, including the elongation of the distance between the pulse compressor gratings, leading to the elongation of the pulse duration[31]. Laser-beam drift, which degrades the signal of the pump-induced dynamics, was also detected within ~8 h, although the origin of this drift was not identified.

The present technique is a type of 2D imaging, limiting the information in 3D. In the case of a Coulomb explosion, only the fragment of ions ejected in the detection plane contribute to the image. This implies that it is difficult to apply the present method directly to complicated fragmentation processes, such as those involved in coincidence imaging studies[25,32,33]. We note that the sum of the signal intensity with our method is proportional to the probability in the detection plane. This represents indirect information on the dimension not included in the imaging plane[11,12].

While we focus on Coulomb explosion imaging in this paper, the present approach can be, in principle, applied to general charged-particle imaging, such as that involved in photodissociation studies[14]. In the existing imaging procedure, to obtain a 2D tomogram of a 3D Newton sphere of charged particles, the polarization of light should be parallel to the detector surface. In other words, the camera angle is limited to particular conditions. Also, in the present 2D imaging technique, a 3D ion cloud is spatially sliced to a 2D cut and is then imaged. With this slice imaging, the freedom of the camera angle will open a way to obtain hitherto-unobserved information that sometimes appears in the laser propagation direction[26,34].

Disclosures

The authors have nothing to disclose.

Acknowledgements

This work was supported in part by grants-in-aid KAKENHI from the Japan Society for the Promotion of Science (JSPS) and the Ministry of Education, Culture, Sports, Science, and Technology (MEXT) Japan (#26104539, #26620020, #26810011, #15H03766, #15KT0060, #16H00826, and #16K13927); the Konica Minolta Science and Technology Foundation; the "Planting Seeds for Research" program of TokyoTech; the Imaging Science Project of the Center for Novel Science Initiatives (CNSI) at the National Institutes of Natural Sciences (NINS) (#IS261006); the RIKEN-IMS joint program on "Extreme Photonics;" and the Consortium for Photon Science and Technology (CPhoST).

References

1. Stapelfeldt, H., Constant, E., Sakai, H., & Corkum, P. B. Time-resolved Coulomb explosion imaging: A method to measure structure and dynamics of molecular nuclear wave packets. *Phys. Rev. A.* **58**, 426-433, (1998).
2. Hishikawa, A., Matsuda, A., Fushitani, M., & Takahashi, E. J. Visualizing Recurrently Migrating Hydrogen in Acetylene Dication by Intense Ultrashort Laser Pulses. *Phys. Rev. Lett.* **99**, 258302, (2007).
3. Légaré, F. *et al.* Laser Coulomb-explosion imaging of small molecules. *Phys. Rev. A.* **71**, 013415, (2005).
4. Stapelfeldt, H., & Seideman, T. Colloquium: Aligning molecules with strong laser pulses. *Rev. Mod. Phys.* **75**, 543-557, (2003).
5. Ohshima, Y., & Hasegawa, H. Coherent rotational excitation by intense nonresonant laser fields. *Int. Rev. Phys. Chem.* **29**, 619-663, (2010).
6. Kitano, K., Hasegawa, H., & Ohshima, Y. Ultrafast Angular Momentum Orientation by Linearly Polarized Laser Fields. *Phys. Rev. Lett.* **103**, 223002, (2009).
7. Fleischer, S., Khodorkovsky, Y., Prior, Y., & Averbukh, I. S. Controlling the sense of molecular rotation. *New J. Phys.* **11**, 105039, (2009).
8. Korobenko, A., Milner, A. A., & Milner, V. Direct Observation, Study, and Control of Molecular Superrotors. *Phys. Rev. Lett.* **112**, 113004, (2014).

9. Rosca-Pruna, F., & Vrakking, M. J. J. Revival structures in picosecond laser-induced alignment of I_2 molecules. I. Experimental results. *J. Chem. Phys.* **116**, 6567-6578, (2002).
10. Dooley, P. W. *et al.* Direct imaging of rotational wave-packet dynamics of diatomic molecules. *Phys. Rev. A.* **68**, 023406, (2003).
11. Mizuse, K., Kitano, K., Hasegawa, H., & Ohshima, Y. Quantum unidirectional rotation directly imaged with molecules. *Sci. Adv.* **1**, e1400185 (2015) .
12. Lin, K. *et al.* Visualizing molecular unidirectional rotation. *Phys. Rev. A.* **92**, 013410, (2015).
13. Korobenko, A., Hepburn, J. W., & Milner, V. Observation of nondispersing classical-like molecular rotation. *Phys. Chem. Chem. Phys.* **17**, 951-956, (2015).
14. Whitaker, B. J. *Imaging in Molecular Dynamics.* Cambridge University Press, (2003).
15. Ullrich, J. *et al.* Recoil-ion and electron momentum spectroscopy: reaction-microscopes. *Rep. Prog. Phys.* **66**, 1463, (2003).
16. Lee, S. K. *et al.* Coincidence ion imaging with a fast frame camera. *Rev Sci Instrum.* **85**, 123303, (2014).
17. Lee, S. K. *et al.* Communication: Time- and space-sliced velocity map electron imaging. *J. Chem. Phys.* **141**, 221101, (2014).
18. John, J. J. *et al.* PImMS, a fast event-triggered monolithic pixel detector with storage of multiple timestamps. *Journal of Instrumentation.* **7**, C08001, (2012).
19. Nomerotski, A. *et al.* Pixel Imaging Mass Spectrometry with fast and intelligent Pixel detectors. *Journal of Instrumentation.* **5**, C07007-C07007, (2010).
20. Luria, K., Christen, W., & Even, U. Generation and Propagation of Intense Supersonic Beams. *J. Phys. Chem. A.* **115**, 7362-7367, (2011).
21. Eppink, A. T. J. B., & Parker, D. H. Velocity map imaging of ions and electrons using electrostatic lenses: Application in photoelectron and photofragment ion imaging of molecular oxygen. *Rev. Sci. Instrum.* **68**, 3477-3484, (1997).
22. Gebhardt, C. R., Rakitzis, T. P., Samartzis, P. C., Ladopoulos, V., & Kitsopoulos, T. N. Slice imaging: A new approach to ion imaging and velocity mapping. *Rev. Sci. Instrum.* **72**, 3848, (2001).
23. Stöhr, J. *NEXAFS Spectroscopy.* 132 Springer, (1992).
24. Siders, C. W., Siders, J. L. W., Taylor, A. J., Park, S.-G., & Weiner, A. M. Efficient High-Energy Pulse-Train Generation Using a 2 n-Pulse Michelson Interferometer. *Appl. Opt.* **37**, 5302-5305, (1998).
25. Pitzer, M. *et al.* Direct Determination of Absolute Molecular Stereochemistry in Gas Phase by Coulomb Explosion Imaging. *Science.* **341**, 1096-1100, (2013).
26. Rakitzis, T. P., Samartzis, P. C., & Kitsopoulos, T. N. Observing the symmetry breaking in the angular distributions of oriented photofragments using velocity mapping. *J. Chem. Phys.* **111**, 10415, (1999).
27. Chang, B.-Y., Hoetzlein, R. C., Mueller, J. A., Geiser, J. D., & Houston, P. L. Improved two-dimensional product imaging: The real-time ion-counting method. *Rev. Sci. Instrum.* **69**, 1665, (1998).
28. Wiley, W. C., & McLaren, I. H. Time-of-Flight Mass Spectrometer with Improved Resolution. *Rev. Sci. Instrum.* **26**, 1150, (1955).
29. Townsend, D., Minitti, M. P., & Suits, A. G. Direct current slice imaging. *Rev. Sci. Instrum.* **74**, 2530, (2003).
30. Wu, G. *et al.* A new crossed molecular beam apparatus using time-sliced ion velocity imaging technique. *Rev. Sci. Instrum.* **79**, 094104, (2008).
31. Treacy, E. Optical pulse compression with diffraction gratings. *Quantum Electronics, IEEE Journal of.* **5**, 454-458, (1969).
32. Dörner, R. et al. Cold Target Recoil Ion Momentum Spectroscopy: a 'momentum microscope' to view atomic collision dynamics. *Physics Reports.* **330**, 95-192, (2000).
33. Herwig, P. *et al.* Imaging the Absolute Configuration of a Chiral Epoxide in the Gas Phase. *Science.* **342**, 1084-1086, (2013).
34. Suzuki, Y.-I., & Suzuki, T. Linear and circular dichroism in photoelectron angular distributions caused by electron correlation. *Phys. Rev. A.* **91**, 053413, (2015).

